search," *Proc. Conf. Computer Aided Design of Electronic, Microwave Circuits and Systems*, Hull, England, pp. 72–77, July 1977.
[3] ——, "Generalized worst case design, with applications to microwave networks" (in Dutch), Ph.D. dissertation, Faculty of Engineering, University of Ghent, Ghent, Belgium, May 1978.
[4] J. W. Bandler, P. C. Liu, and J. H. K. Chen, "Worst case network tolerance optimization," *IEEE Trans. Microwave Theory Tech.*, vol. MTT-23, pp. 630–641, Aug. 1975.
[5] J. W. Bandler, P. C. Liu, and H. Tromp, "A nonlinear programming approach to optimal design centering, tolerancing, and tuning," *IEEE Trans. Circuits Syst.*, vol. CAS-23, pp. 155–165, Mar. 1976.
[6] J. F. Pinel and K. A. Roberts, "Tolerance assignment in linear networks using nonlinear programming," *IEEE Trans. Circuit Theory*, vol. CT-19, pp. 475–479, Sept. 1972.

An Approximate Dynamic Spatial Green's Function for Microstriplines

Y. LEONARD CHOW, MEMBER, IEEE, AND IBRAHIM N. EL-BEHERY

***Abstract*—A dynamic model of both charge and current images is constructed to give rise to a frequency-dependent dyadic Green's function in the space domain for microstriplines. While the spatial Green's function is approximate, its image model is very simple, and the propagation constants calculated from it agree well with published results.**

I. Introduction

THE DYADIC Green's function in the spectral domain for microstriplines has been derived by Denlinger [1]. The expression of this Green's function, however, while being exact, is quite complicated making its use difficult in arbitrarily shaped structures.

The dyadic Green's function in the space domain, on the other hand, may overcome this difficulty, but it is generally not known in a closed form. A static equivalent, however, has been derived by Silvester [2] from a model of charge images. The simplicity of this model and the good physical insight it gives naturally suggest the possibility of its extension to a dynamic model that can reasonably approximate the dyadic Green's function at the higher frequencies.

While such an approach may be used to construct dynamic Green's functions in three dimensions for arbitrarily shaped microstrip structures, this paper, being a first attempt in this direction, considers only the extension to the Green's function in two dimensions for microstriplines.

In this paper the two-dimensional Green's function is defined as the kernel function of the integral equation

Manuscript received May 29, 1978; revised July 28, 1978. This work was supported in part by the Communications Research Center of Canada through the Department of Supply and Services under Contract 08SU. 36100-7-9511 and in part by the National Research Council of Canada under Grant A3804.

The authors are with the Department of Electrical Engineering, University of Waterloo, Waterloo, Ont. N2L 3G1, Canada.

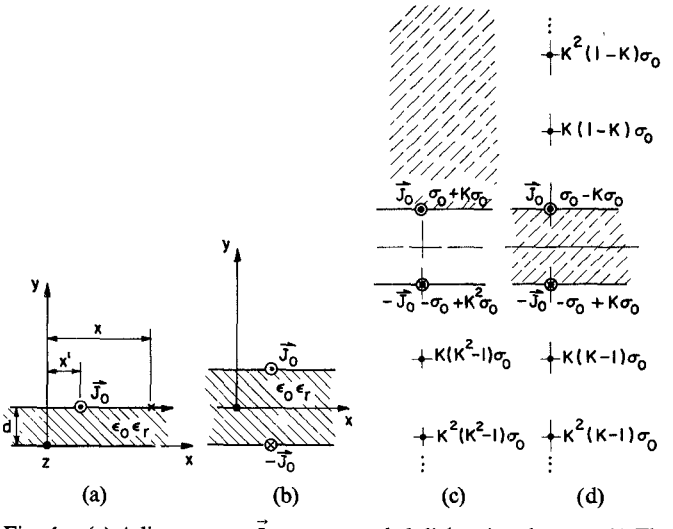

Fig. 1. (a) A line current $\vec{J}_0$ on a grounded dielectric substrate. (b) The equivalent of (a): a dielectric substrate with two true currents. (c) The model for the outside (dashed) region with true currents and charges $\pm\vec{J}_0$ and $\pm\sigma_0$ and image charges σ_n. The magnitudes of the images are indicated with $K=(1-\epsilon_r)/(1+\epsilon_r)$. The separation between adjacent images is $2d$. (d) The model for the inside (dashed) region.

$$\vec{E}_{\tan}(x)=\int \bar{\bar{G}}(x,x')\cdot\vec{J}_0(x')dx' \tag{1}$$

where, according to the geometry of Fig. 1(a),

$$\bar{\bar{G}}(x,x')=\begin{bmatrix} G_{xx}(x,x') & G_{xz}(x,x') \\ G_{zx}(x,x') & G_{zz}(x,x') \end{bmatrix} \tag{2}$$

and where $\vec{J}_0(x)$ and $\vec{E}_{\tan}(x)$ are, respectively, the density of the current vector and the tangential electric field vector on the surface of the grounded dielectric substrate of Fig. 1(a).

0018-9480/78/1200-0978$00.75 ©1978 IEEE

II. The Dynamic Model for the Dyadic Green's Function

By simple reflection from the conducting ground plane, the configuration of Fig. 1(a) can be replaced by its electrical equivalent shown in Fig. 1(b). In the latter we have two parallel currents, $\vec{J}_0$ and its reflection $-\vec{J}_0$, bracketing a substrate twice the original in thickness.

Under a static condition there is no electric field, and, according to the Biot–Savart law, the magnetic field distribution generated by $\vec{J}_0$ and $-\vec{J}_0$ is not affected by the presence of the dielectric substrate. When the currents begin to oscillate slowly, however, two types of electric fields appear. The first type is due to the changing magnetic field according to Faraday's law. As Faraday's law is not dependent on the medium dielectric constant, this electric field distribution is again not affected by the presence of the dielectric substrate. This means that this type of electric field is accounted for by the two true currents alone without any current images from the dielectric boundaries in Fig. 1(b).

The second type of electric field is due to the charges σ_0 and $-\sigma_0$ generated by the oscillating currents $\vec{J}_0$ and $-\vec{J}_0$ through the continuity equation

$$-j\omega\sigma_0 = \nabla\cdot\vec{J}_0. \tag{3}$$

This type of electric field is affected by the presence of the dielectric substrate. To satisfy the boundary condition on the tangential electric fields, therefore, according to Silvester [2], one may assume that they are generated by two series of charge images $\sigma_n (n=1,2,\cdots)$ in addition to the true charges σ_0 and $-\sigma_0$. One series is for the field outside the dielectric substrate and the other for the field inside the substrate, as shown in Figs. 1(c) and (d).

According to the above and for propagating currents with a phase factor $e^{-jk_z z}$, the net electric field is the sum of the above two types of fields, i.e.,

$$\vec{E} = -j\omega\mu_0\left(\vec{A}_0^+ + \vec{A}_0^-\right) - \nabla\left[\phi_0^+ + \phi_0^- + \sum_{n=1}^{\infty}\phi_n\right] \tag{4}$$

where, in the first type, the vector potentials $\vec{A}_0^+$ and $\vec{A}_0^-$ are obtained from the true currents $\vec{J}_0$ and $-\vec{J}_0$ through

$$\vec{A}_0(\vec{\rho}) = \frac{1}{4j}\int H_0^{(2)}(k_t|\vec{\rho}-\vec{\rho}'|)\vec{J}_0(\vec{\rho}')d\vec{\rho}' \tag{5}$$

and where, in the second type, the scalar potentials ϕ_0^+, ϕ_0^-, and ϕ_n are obtained from the true charges σ_0, $-\sigma_0$, and their images σ_n by

$$\phi_i(\vec{\rho}) = \frac{1}{4j\epsilon}\int H_0^{(2)}(k_t|\vec{\rho}-\vec{\rho}'|)\sigma_i(\vec{\rho}')d\vec{\rho}', \qquad i=0,1,2,\cdots \tag{6}$$

where $\vec{\rho}$ is the radius vector, ϵ is the permittivity of the region being considered, k_t is the corresponding propagation constant in the transverse xy plane, and $H_0^{(2)}$ is a Hankel function of the second kind.

III. Limits and Justification of the Dynamic Model

The electric field in [4] is obtained through the fundamental laws of Biot–Savart, Faraday, the continuity equation, and Coulomb, under low-frequency conditions. Evidently, therefore, the electric field must reasonably satisfy the tangential boundary condition on the dielectric–air interface for the relatively short distances normally encountered in microstrip structures, i.e., distances, say, less than $\lambda/8$ in the dielectric.

More rigorously, however, it can be shown that the electric field in (4) satisfies the four Maxwell's equations in differential form provided that the Lorentz condition [3] is defined as

$$\nabla\cdot\left(\vec{A}_0^+ + \vec{A}_0^-\right) + j\omega\epsilon\left[\phi_0^+ + \phi_0^- + \sum_{n=1}^{\infty}\phi_n\right] = 0. \tag{7}$$

It is to be noticed that while the continuity equation applies to the true charge and current pairs $(\sigma_0, \vec{J}_0)$ and $(-\sigma_0, -\vec{J}_0)$, it does not apply to the charge images σ_n as there are no corresponding current images. This does not present a problem, however, since the images do not physically exist. They are introduced only as a mathematical convenience to simplify the field representation inside the region being considered while they themselves are located outside.

IV. The Dyadic Green's Function

Assuming $\vec{J}_0$ to be a unit line current with the line directed along the z axis, the components of the dyadic Green's can easily be obtained from (3) to (6). In these equations, if the unit current $\vec{J}_0$ is in the x direction, the x and z components of the electric field on the surface of the substrate give G_{xx} and G_{xz}, respectively. Similarly taking the unit current $\vec{J}_0$ in the z direction leads to G_{xz} and G_{zz}.

It can easily be observed from (4) and (6) that the cross components are equal, i.e., $G_{xz} = G_{zx}$. Therefore, only three elements in the 2×2 matrix of the dyadic Green's function need be computed. It may also be of interest to notice from (4) that the cross components are due to the electric field of the second type only, i.e., they are generated from the scalar potentials ϕ only.

The detailed expressions for the components G_{xx}, G_{xz}, and G_{zz} are given in Appendix A. These components are plotted in Fig. 2 as functions of the distance along the surface of the dielectric substrate. The plots show the magnitudes of the components calculated for outside and inside the dielectric. As can be seen, the outside and inside Green's function match well in the region of interest, i.e., less than $\lambda/8$ inside the dielectric, or $x < 7d$ in Fig. 2. They deviate appreciably from each other, however, for larger distances. Comparisons are made, therefore, between the outside and inside Green's functions with the exact values obtained from Denlinger's spectral-domain Green's function by Fourier transform. The com-

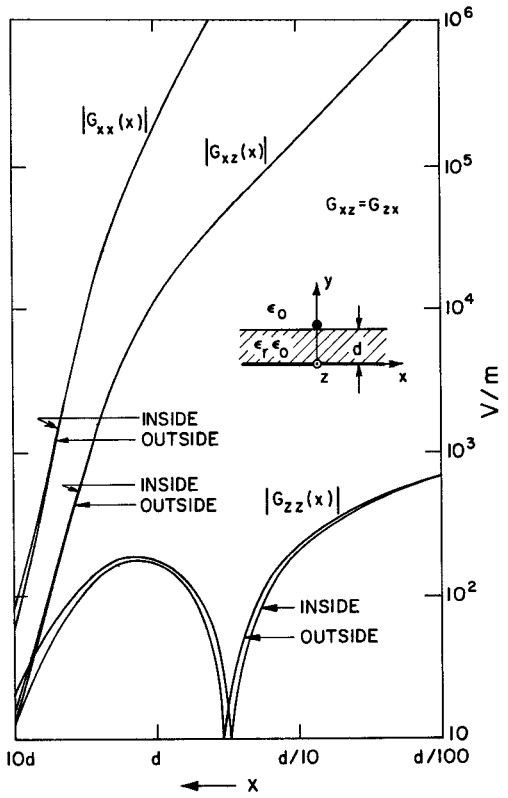

Fig. 2. The tangential components of the two dyadic Green's functions, inside and outside the dielectric substrate at $k_z=0.88\sqrt{\epsilon_r}k_0$, $\epsilon_r=3, d=3$ mm, and $f=1$ GHz.

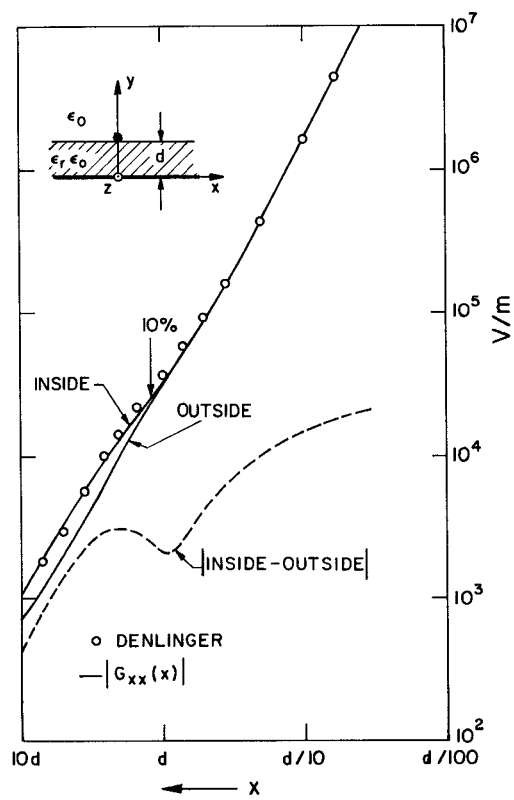

Fig. 3. A comparison between the Green's function components G_{xx} and that transformed from Denlinger's at $k_z=0, \epsilon_r=3, d=3$ mm, and $f=10$ GHz. The point of 10-percent difference between inside and outside is indicated.

parison shows that the inside Green's function appears to be closer to the exact values than the outside one, as shown in the example in Fig. 3. For this reason, the inside Green's function is used in the example below.

V. Propagation Constants of Microstriplines

A good test for the validity of the Green's function of the dynamic model is whether it can produce the frequency dispersion characteristics in the propagation constants of microstriplines which cannot be obtained by the Green's functions of the static model.

To this end we use the inside Green's function in (1) and apply the latter to the conducting surface of a microstripline. If we take the origin to be at the center of the conducting strip and denote the latter's width by w, then (1) becomes

$$\vec{E}_{\tan}(x)=\int_{-w/2}^{w/2}\bar{\bar{G}}(x-x')\cdot\vec{J}_0(x')dx' \tag{8}$$

in which the unknown are the propagation constant $k_z=\sqrt{\omega^2\mu_0\epsilon_0\epsilon_r-k_t^2}$ and the current density $\vec{J}_0$ on the strip.

To solve (8) numerically, we use the point-matching moment method in which the conducting strip is divided into $2N$ equal segments, each of width Δ. If we let $\vec{E}_{\tan}(x)=\hat{x}E_x+\hat{z}E_z$ and $\vec{J}_0(x)=\hat{x}J_x+\hat{z}J_z$, where $\hat{x}$ and $\hat{z}$ are unit vectors on the conducting strip, and if we notice the symmetries $J_z(x)=J_z(-x)$ and $J_x(x)=-J_x(-x)$, then (8) can be expanded in terms of positive x only.

$$E_z(x)=\sum_{i=1}^{N}\int_{x_i-\Delta/2}^{x_i+\Delta/2}\left[\{G_{zz}(x-x')+G_{zz}(x+x')\}J_z(x')+\{G_{zx}(x-x')-G_{zx}(x+x')\}J_x(x')\right]dx' \tag{9}$$

and

$$E_x(x)=\sum_{i=1}^{N}\int_{x_i-\Delta/2}^{x_i+\Delta/2}\left[\{G_{xz}(x-x')+G_{xz}(x+x')\}J_z(x')+\{G_{xx}(x-x')-G_{xx}(x+x')\}J_x(x')\right]dx' \tag{10}$$

where x_i, $i=\pm1,\cdots,\pm N$ are the center points of the segments. When the segment width Δ is sufficiently small, one can approximate the integral over the ith segment at a point x_p, $p\neq i$, by assuming the current density and the Green's function to be of constant values over the segment. When $i=p$, however, the integral (self-term) must be evaluated since the Green's function becomes unbounded. This can be accomplished by taking the current density to be uniform and assuming the conducting strip to have a small but finite thickness. Expressions for the integrals in (9) and (10) and the details of their evaluation are given in Appendix B.

By matching the electric field at the center points x_p, $p=1,\cdots,N$ to zero we obtain a set of linear homogeneous equations of the form

$$\bar{\bar{\Gamma}}\cdot\vec{I}=\vec{0} \tag{11}$$

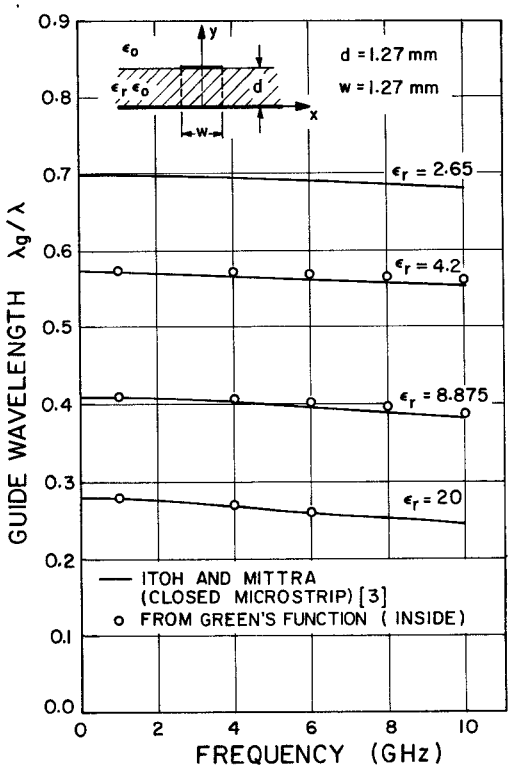

Fig. 4. The guide wavelengths of the microstripline at different ϵ_r as a function of frequency; a comparison between those of Itoh and Mittra and those from the inside spatial Green's function.

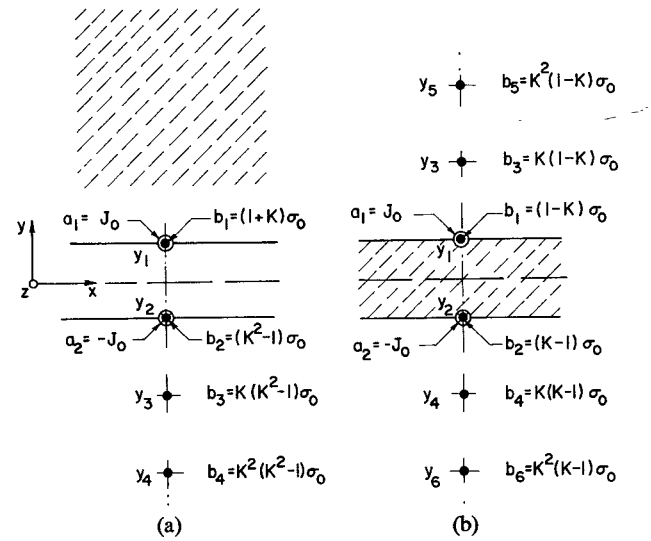

Fig. 5. A numbering system for the set of currents and charges (true and/or image) of the dynamic model for (a) the region outside the dielectric and (b) the region inside the dielectric.

where $\bar{\bar{\Gamma}}$ is a $2N \times 2N$ matrix depending on k_z, and $\vec{I}$ a column vector whose components are the surface currents in the x and z directions on each segment. For (11) to have a nontrivial solution, the determinant of $\bar{\bar{\Gamma}}$ must vanish, i.e.,

$$\|\bar{\bar{\Gamma}}(k_z)\| = 0. \tag{12}$$

The solution of (12) provides the required value of k_z.

The dispersion results which are obtained using $N=2$ are shown in Fig. 4 in terms of the ratio of the guide to the free-space wavelengths at different frequencies, for various dielectric constants of the substrate. The figure also shows the corresponding results given in Itoh and Mittra [4] for comparison. As observed, the agreement is good for the range of parameters considered.

Finally a word about the computing time. It can be shown that in Green's function expressions (4), the infinite series converges considerably faster than a geometric series. For ϵ_r between 3 and 20, about 20–80 terms are required to achieve a 6-decimal-place accuracy. Using an IBM 370/158 machine, this means that the computing time required to obtain a single point in Fig. 4 is between 0.5–2 s depending on the relative permitivity of the substrate used.

VI. Conclusion

The dynamic model of current and charge images proves to be a good approximation for the spatial dyadic Green's function of microstriplines; the crucial test has been its capability of showing the small frequency dispersion in the propagation constants of microstriplines. Because the model is simple, the computer program is easy to write, and, as shown in the example, the computer time is short.

The model fails, however, outside the normal range of parameters where surface waves play a dominant part since the model does not take them into account.

While the Green's function derived here is in two dimensions, the dynamic model is evidently valid for both two and three dimensions similar to the static model by Silvester [2], [5]. It is believed, therefore, that this model can be used to generate the three-dimensional Green's function for the frequency dependent properties of arbitrarily shaped microstrip structures.

It may be added that while the computer time is short in calculating the propagation constants using the spatial Green's function, it may or may not be shorter than that using the spectral Green's function. An example of the latter may be that with carefully chosen moment-method expansion functions, recently by Jansen [6]. Nevertheless, the spectral Green's function is very complicated; therefore, its application to the arbitrarily shaped microstrip structures may be more difficult than the application with the spatial Green's function.

Appendix A
Expressions of the Dyadic Green's Function

To put the Green's function in a simple form suitable for computational purposes, we adopt a numbering system which orders the set of currents and charges of the dynamic model for the regions outside and inside the dielectric, in the manner shown in Fig. 5. In this figure a_n and b_n denote the amplitudes of the nth line current and line charge (true and/or image) located at the distance y_n along the y axis from the origin.

According to this system, the components of the Green's function for both the outside and the inside

regions are expressed in the form

$$G_{xx}(x,x')=\left[\sum_{n=1}^{2} a_n g^A_{xx,n}+\sum_{n=1}^{\infty} b_n g^{\phi}_{xx,n}\right]e^{-jk_z z} \quad \text{(A1)}$$

$$G_{xz}(x,x')=\left[\sum_{n=1}^{\infty} b_n g^{\phi}_{xz,n}\right]e^{-jk_z z} \quad \text{(A2)}$$

$$G_{zx}(x,x')=G_{xz}(x,x') \quad \text{(A3)}$$

$$G_{zz}(x,x')=\left[\sum_{n=1}^{2} a_n g^A_{zz,n}+\sum_{n=1}^{\infty} b_n g^{\phi}_{zz,n}\right]e^{-jk_z z} \quad \text{(A4)}$$

where the g^A_n and g^{ϕ}_n functions are, respectively, the vector and scalar potentials of the nth current and charge sources as derived from (4)–(6). Specifically, the g's are

$$g^A_{xx,n}=-j\omega\mu_0 A_x(\rho_n)=-\frac{\omega\mu_0}{4}H_0^{(2)}(k_t\rho_n) \quad \text{(A5)}$$

and

$$g^A_{zz,n}=-j\omega\mu_0 A_z(\rho_n)=g^A_{xx,n} \quad \text{(A6)}$$

where

$$k_t=\left(k_z^2-\omega^2\mu_0\epsilon\right)^{1/2} \quad \text{(A7)}$$

$$\rho_n=\left[(x-x')^2+(y_n-d)^2\right]^{1/2}. \quad \text{(A8)}$$

$A_x(\rho_n)$ and $A_z(\rho_n)$ are vector potentials of unit line currents at the location (x',y_n) and pointing in the respective x and z directions, d is the thickness of the grounded dielectric substrate, and ϵ is the permittivity of the medium equaling to $\epsilon_0\epsilon_r$ inside the dielectric and to ϵ_0 outside.

For the g^{ϕ}'s we have

$$g^{\phi}_{xx,n}=\frac{-\partial}{\partial x}\phi_x(\rho_n)=\frac{k_t^2}{4\omega\epsilon}\left[\frac{(x-x')^2}{\rho_n^2}H_0^{(2)}(k_t\rho_n)+\frac{1}{k_t\rho_n}\left\{1-2\frac{(x-x')^2}{\rho_n^2}\right\}H_1^{(2)}(k_t\rho_n)\right] \quad \text{(A9)}$$

$$g^{\phi}_{xz,n}\left(=g^{\phi}_{zx,n}\right)=-\frac{\partial}{\partial x}\phi_z(\rho_n)=-j\frac{k_z k_t}{4\omega\epsilon}\frac{x-x'}{\rho_n}H_1^{(2)}(k_t\rho_n) \quad \text{(A10)}$$

$$g^{\phi}_{zz,n}=-\frac{\partial}{\partial z}\phi_z(\rho_n)=\frac{k_z^2}{4\omega\epsilon}H_0^{(2)}(k_t\rho_n) \quad \text{(A11)}$$

where $\phi_x(\rho_n)$ and $\phi_z(\rho_n)$ are the scalar potentials derived from the charges, generated according to (3) and Fig. 5 from the true currents pointing in the respective x and z directions. The true currents are located at (x',y_n), $n=1,2$.

It is to be noted that for microstrip applications, the propagation constant k_t in the transverse plane becomes imaginary for the region outside the dielectric. In this case the Hankel functions $H_0^{(2)}$ and $H_1^{(2)}$ become modified Bessel functions of the second kind.

Appendix B
Evaluation of the Integrals in (9) and (10)

Through substitutions of (A1)–(A4), the integrals in (9) and (10) can be reduced to a sum of integrals of the following basic form:

$$S^C_{\alpha\beta,n}(x_i,x_p)=\int_{x_i-\Delta/2}^{x_i+\Delta/2} g^C_{\alpha\beta,n}(x-x_p,y_n)J_\beta(x)dx \quad \text{(B1)}$$

where x_p is the field matching point at the center of the pth segment, (x_i,y_n) are the coordinates of the source point (according to Fig. 5, the nth source, current or charge), the superscript $C=A$ or ϕ, and the subscripts $\alpha,\beta=x$ or z.

When $i\neq p$ or $n\neq 1$ (i.e., $y_n\neq d$ in Fig. 5), $g^c_{\alpha\beta,n}$ and $J_\beta(x)$ can be considered to be constant over the segment width Δ when the latter is sufficiently small. Equation (B1) may thus be approximated to

$$S^C_{\alpha\beta,n}(x_i,x_p)=g^C_{\alpha\beta,n}(x_i-x_p,y_n)I_{\beta i} \quad \text{(B2)}$$

where

$$I_{\beta i}=J_\beta(x_i)\cdot\Delta. \quad \text{(B3)}$$

When $i=p$ and $n=1$ (i.e., $y_n=d$), (B1) becomes the self-term and the approximation (B2) diverges. An alternative evaluation of (B1) must therefore be used. If the current density $J_\beta(x)$ can be assumed to be constant over the segment width (i.e., when J_β is known *a priori* to be bounded on the segment) the resulting integral can then be treated in one of three different ways depending on the type of the g-function involved.

First we consider $S^{\phi}_{zx,1}$. From (A10) it is seen that $g^{\phi}_{zx,1}$ is skew-symmetric about the center of the segment; it follows,therefore, that

$$S^{\phi}_{zx,1}(x_i,x_i)=0. \quad \text{(B4)}$$

Next we consider $S^A_{\alpha\alpha,1}$ and $S^{\phi}_{zz,1}$. These, according to (A5), (A6), and (A11) are integrals of the Hankel function $H_0^{(2)}$ over small arguments, the approximate evaluation of which are well known from Harrington [7] and are given by

$$S^A_{\alpha\alpha,1}(x_i,x_i)=\frac{-\omega\mu_0}{4}D\cdot I_{\alpha i}, \qquad \alpha=x \text{ or } z \quad \text{(B5)}$$

$$S^{\phi}_{zz,1}(x_i,x_i)=\frac{k_z^2}{4\omega\epsilon}D\cdot I_{zi} \quad \text{(B6)}$$

where

$$D=A_1+A_2\cdot\left[-1+\ln\left(k_t\frac{\Delta}{2}\right)\right] \quad \text{(B7)}$$

$$A_1=1-j\left(0.367\,467-\frac{2}{\pi}\ln 2\right) \quad \text{and} \quad A_2=-j\frac{2}{\pi}.$$

In the third case we have $S^{\phi}_{xx,1}$. From (A9) we can see that the integrand $g^{\phi}_{xx,1}$ is an x derivative of $\phi_x(\rho_1)$. The integral, therefore, diverges since $\phi_x(0)$ is unbounded. To avoid this situation, we assume that the conducting strip has a small but finite thickness t and that the current sheet

J_x is concentrated at the center of the conductor so that its separation from the boundary is $t/2$. The integral converges as a result and assumes the value

$$S^{\phi}_{xx,1}(x_i,x_i)=\frac{k_t}{4\omega\epsilon}H_1^{(2)}\left(k_t\frac{\Delta}{2}\right)\cdot\frac{2}{\Delta}I_{xi} \tag{B8}$$

which is independent of t provided that $t\ll\Delta$.

Finally, when a current density $J_\beta(x)$ is unbounded on a segment, as is the case for $J_z(x)$ at the edges of the conducting strip, the validity of its approximation by a constant value should be examined. The two integrals which concern us then are $S^{c}_{zz,1}$ and $S^{\phi}_{xz,1}$ evaluated on an edge segment. Under the approximation of the constant current density, the first integral has the finite value given in (B6) while the second integral vanishes as in (B4). We may assume that the error introduced in the first integral is smaller than its true value and can thus be neglected. The error introduced in the second integral, however, is equal to its true value and may not, therefore, be ignored. To evaluate $S^{\phi}_{xz,1}$ on an edge segment, we assume a current density J_z that satisfies the edge condition. We may thus write

$$J_z(x)=\frac{1}{2}\left[\Delta\left(\frac{\Delta}{2}-x\right)\right]^{-1/2}I_{zN}. \tag{B9}$$

Using (B9) in (B1) and applying the small argument approximation of the function $H_1^{(2)}$, we arrive, after the evaluation of some standard integrals, at the result

$$S^{\phi}_{xz,1}(x_N,x_N)=-j\frac{k_z k_t}{4\omega\epsilon}\frac{1}{2}FI_{zN} \tag{B10}$$

where

$$F=j\sqrt{2}\,\frac{0.6366}{k_t\Delta}\ln(3-2\sqrt{2}). \tag{B11}$$

References

[1] E. J. Denlinger, "A frequency dependent solution for microstrip transmission lines," *IEEE Trans. Microwave Theory Tech.*, vol. MTT-19, pp. 30–39, Jan. 1971.

[2] P. Silvester, "TEM wave properties of microstrip transmission lines," *Proc. Inst. Elec. Eng.*, vol. 115, pp. 43–48, Jan. 1968.

[3] R. E. Collin, *Field Theory of Guided Waves*. New York: McGraw-Hill, 1960, pp. 23.

[4] T. Itoh and R. Mittra, "Spectral-domain approach for calculating dispersion characteristics of microstrip lines," *IEEE Trans. Microwave Theory Tech.*, vol. MTT-21, pp. 496–499, July 1973.

[5] P. Benedek and P. Silvester, "Microstrip discontinuity capacitances for right-angle bends, T-junctions, and crossings," *IEEE Trans. Microwave Theory Tech.*, vol. MTT-21, pp. 341–346, May 1973.

[6] R. H. Jansen, "High-speed computation of single and coupled microstrip parameters including dispersion, high-order modes, loss, and finite strip thickness," *IEEE Trans. Microwave Theory Tech.*, vol. MTT-26, pp. 75–82, Feb., 1978.

[7] R. F. Harrington, *Field Computation by Moment Methods*. New York: MacMillan, 1968, pp. 44.

Generalized Spectral Domain Method for Multiconductor Printed Lines and Its Application to Turnable Suspended Microstrips

TATSUO ITOH, SENIOR MEMBER, IEEE

Abstract—**An efficient method is developed for obtaining propagation characteristics of microstripline type structures in which a number of conductors are located on various interfaces. Specific computations have been carried out for suspended microstripline structures with tuning conductive septums. A number of data useful for design are included.**

Manuscript received April 20, 1978; revised July 31, 1978. This work was supported in part by U.S. Army Research Grants DAAG29-77-G-0220 and DAAG29-78-G-0146.

The author is with the Department of Electrical Engineering, University of Texas, Austin, TX 78712.

I. Introduction

THE SPECTRAL domain technique developed by Itoh and Mittra has been applied to a number of microstripline structures [1], [2]. It is an efficient numerical technique having several advantages over many other methods [3], [4]. However, to date, this technique has been applied only to the structures in which center conductors (strips) are located on one of the dielectric interfaces, e.g., the air-substrate interface.

0018-9480/78/1200-0983$00.75 ©1978 IEEE